Inorganic Chemistry

Article

pubs.acs.org/IC

Coupling XRD, EXAFS, and ^{13}C NMR to Study the Effect of the Carbon Stoichiometry on the Local Structure of $UC_{1\pm x}$

U. Carvajal Nuñez,*[,†] L. Martel,[†] D. Prieur,[†] E. Lopez Honorato,[‡] R. Eloirdi,[†] I. Farnan,[§] T. Vitova,[∥] and J. Somers[†]

[†]European Commission, Joint Research Centre, Institute for Transuranium Elements, P.O. Box 2340, D-76125 Karlsruhe, Germany

[‡]CINVESTAV, Unidad Saltillo Carretera Saltillo-Monterrey, Km 13.5, Ramos Arizpe 25900, Coahuila, México

[§]University of Cambridge, Cambridge CB2 1TN, United Kingdom

[∥]Institut für Nukleare Entsorgung (INE), P.O. Box 3640, D-76021 Karlsruhe, Germany

ABSTRACT: A series of uranium carbide samples, prepared by arc melting with a C/U ratio ranging from 0.96 to 1.04, has been studied by X-ray diffraction (XRD), ^{13}C nuclear magnetic resonance (NMR), and extended X-ray absorption fine structure (EXAFS). XRD determines phase uniqueness and the increase of the lattice parameter versus the carbon content. In contrast, ^{13}C NMR detects the different carbon environments in the lattice and in this study, clearly identifies the presence of discrete peaks for carbon in the octahedral lattice site in UC and an additional peak associated with excess carbon in hyperstoichiometric samples. Two peaks associated with different levels of carbon deficiency are detected for all hypostoichiometric compositions. More than one carbon environment is always detected by ^{13}C NMR. This exemplifies the difficulty in obtaining a perfect stoichiometric uranium monocarbide $UC_{1.00}$. The ^{13}C MAS spectra of uranium carbides exhibit the effects resulting from the carbon content on both the broadening of the peaks and on the Knight shift. An abrupt spectral change occurs between hypo- and hyperstoichiometric samples. The results obtained by EXAFS highlight subtle differences between the different stoichiometries, and in the hyperstoichiometric samples, the EXAFS results are consistent with the excess carbon atoms being in the tetrahedral interstitial position.

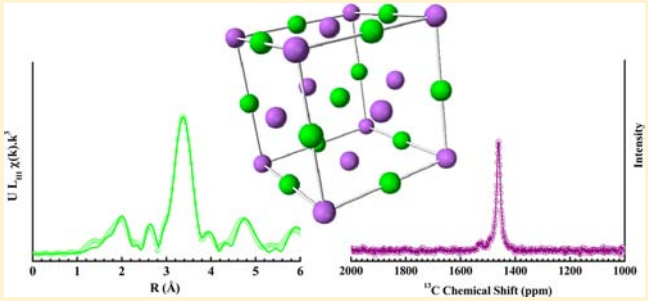

I. INTRODUCTION

A full understanding of nuclear fuels is essential to predict their safe behavior in nuclear power plants. Both characterization and modeling play an important role in this field and thanks to the progress in analytical methods the long-term goal comes closer. Uranium carbides have been widely investigated as advanced nuclear fuels[1] because they present several safety-related advantages compared to oxides fuels.[2] Among others, these materials exhibit a higher thermal conductivity,[3] a higher metal loading, and a lower moderation during irradiation.[4] A higher safety margin is achieved by their operation at about 40% of their melting temperature, in contrast to 80% for oxide fuels.[5−7] Despite these advantages, the use of uranium carbides has been limited because of the difficulties associated with their synthesis.[1] Indeed, the preparation of pure uranium monocarbide, $UC_{1.00}$, is problematic because of its narrow composition limits,[8] and the samples are generally classified in two subgroups, namely, hypo- or hyperstoichiometric carbides samples. In addition, as a result of the carbon loss during the heat treatment, the composition of the sample can vary from one preparation batch to the next, depending on the treatment time and the temperature.[9] Because these carbides are readily oxidized in the presence of humidity, precautions must be taken during their preparation and storage to prevent their degradation.[10,11] Uranium carbides are commonly prepared by either arc melting[12] or carbothermic reduction methods.[13−15] Although arc-melting leads to more homogeneous samples with less oxygen and impurities, the carbothermic reduction is more suitable for large-scale synthesis.[16] Hypo- and hyperstoichiometric uranium carbides compounds, noted hereafter as $UC_{1\pm x}$, crystallize with uranium in the face-centered cubic positions.[8] Two structural types could be envisaged depending on the location of the carbon atoms in the interstices of this structure. These are the NaCl ($Fm\bar{3}m$) or ZnS ($F\bar{4}3m$) types, where the carbon atoms are located in octahedral or tetrahedral sites, respectively.[17] Rundle et al.[18] have reported that carbon atoms in the cubic structure are located in octahedral interstices. This was confirmed by a recent EXAFS study[19] on UC that showed that the ZnS structural model was not consistent with the EXAFS data. In the case of hypostoichiometric carbides, UC_{1-x}, there are vacancies on the octahedral sites of the carbon sublattice. Structural defects,[20] like vacancies or interstitial atoms,[21] affect the material properties of both fresh samples and those during irradiation in reactors, with potential impacts on fuel performance and eventually on the safety of the reactor

Received: August 27, 2013
Published: September 24, 2013

   dx.doi.org/10.1021/ic402144g | *Inorg. Chem.* 2013, 52, 11669−11676

operation. For instance, vacancies lead notably to distortion of the lattice structure and macroscopic swelling,[22] eventually altering material properties such as strength and ductility.

In this study, we report the effect of the carbon content on the ordering of the structure on the atomic scale in uranium carbides $UC_{1\pm x}$ ($0.96 \leq$ "$1 \pm x$" ≤ 1.04). As uranium monocarbide melts incongruently, the samples obtained by arc melting are quenched and are not usually annealed. This quenched state induces some disorder in the lattice, and so far no studies on uranium carbides have reported distributions of vacancies or carbon in the lattice of $UC_{1\pm x}$. Thus, it is essential to evaluate the local environment of the atoms by combining three structural characterization techniques, namely, X-ray diffraction (XRD), nuclear magnetic resonance (NMR), and X-ray absorption spectroscopy (XAS). The new NMR spectrometer at JRC-ITU permits, for the first time, the rapid spinning of the uranium carbide samples and thus high-resolution ^{13}C magic-angle spinning (MAS) spectra. These results are compared to those obtained by EXAFS to provide a detailed atomistic view of the uranium carbide structures.

II. EXPERIMENTAL SECTION

II.1. Sample Preparation and Chemical Analysis. The uranium carbide samples were prepared by the arc melting of the constituent elements, uranium metal, and graphite under a high-purity argon atmosphere (6N) on a water-cooled copper hearth. Metallic zirconium in the chamber acts as a scavenger for oxygen. The $UC_{1\pm x}$ ingots were melted and turned several times to achieve homogeneous samples. The weight losses of the initial charges were below 0.5 wt %. The samples were stored under high vacuum to prevent their oxidation.[23,24] An additional heat treatment was carried out on the $UC_{0.96}$ sample at 1450 °C for 10 h under high vacuum (10^{-5} mbar) followed by a cooling rate of 20 °C/h.

Chemical analyses of the carbon, oxygen, and nitrogen content have been determined by direct combustion using the infrared absorption detection technique with an ELTRA CS-800 instrument.

II.2. X-ray Diffraction. XRD analysis was performed on a Bruker Bragg-Brentano D8 advanced diffractometer (Cu Kα1 radiation) equipped with a Lynxeye linear position sensitive detector. The powder patterns were recorded at room temperature using a step size of 0.01973° with an exposure of 4 s across the angular range $10° \leq 2\theta \leq 120°$. Operating conditions were 40 kV and 40 mA. Lattice parameters were refined by the Le Bail method using the X'Pert HighScore Plus program.

II.3. Nuclear Magnetic Resonance. Uranium carbide ingots were crushed to a fine powder and loaded into 1.3 mm zirconia rotors under helium (6N) in a glovebox. The particle size was sufficiently small to not affect the radiofrequency response of the sample resulting from skin-depth effects. The ^{13}C NMR spectra, with ^{13}C in natural abundance (1.1%), were recorded on a Bruker Advance 400 spectrometer operating at 9.4 T (Larmor frequency of ^{13}C 100 MHz). This apparatus has been adapted for the study of highly radioactive material using commercial NMR probes and rotors.[25] An evacuation tube at the top of the magnet bore is connected via a HEPA filter to the laboratory ventilation system to eliminate the dispersion of radioactive particles in the event of a rotor crash. Despite the potential for eddy current effects during the spinning of the semimetallic uranium carbides, ^{13}C MAS NMR spectra could be acquired at spinning rates of 55 kHz. Rotor-synchronized Hahn echoes were used to acquire the spectra. The pulse durations were 2.5 ($^{\pi}/_{2}$) and 5 μs (π), respectively, with an echo delay of 18.2 μs (1 rotor period). Fully relaxed spectra could be acquired with a relaxation delay of 150 ms because of the paramagnetic relaxation mechanism provided by the conduction electrons.[26] All spectra were calibrated relative to tetramethylsylane (0 ppm) by using adamantane as a secondary reference, with the ^{13}CH and $^{13}CH_2$ peaks at 29.45 and 38.48 ppm,[27] respectively. Because of safety restrictions on running the MAS NMR system unattended overnight, the number of transients was limited to 51 200 for each spectrum. All of the spectra were analyzed and fitted using the dmfit software.[28]

II.4. Extended X-ray Absorption Fine Structure. The uranium carbides ingots were crushed and milled in an agate mortar under a high-purity helium atmosphere (6N) to obtain a small particle size. Five milligrams of powdered samples was mixed with 55 mg of boron nitride, as it is transparent to high-energy X-rays, and then pressed to obtain pellets of about 5 mm in diameter and 1 mm in thickness. Each sample was fixed in a plastic holder and then sealed with Kapton tape in a double bag under an argon atmosphere (6N) and stored in a glass bottle also under an argon atmosphere (6N) up to the measurements made at the ANKA synchrotron site. The samples were observed by optical microscopy and X-ray radiography to characterize the homogeneity of the mixture and the absence of cracks. Furthermore, they were prepared a short time before the experiment to minimize the risk of oxidation.

X-ray absorption spectroscopy (XAS) data were collected at the INE-Beamline at the Angströmquelle Karlsruhe (ANKA).[29] A Ge(422) double-crystal monochromator coupled with a collimating and focusing Rh-coated mirrors was used. XAS spectra were collected in both transmission and fluorescence modes at the U L_{III} (17166 eV) edge. Before averaging the scans, each spectrum was aligned using the Y reference foil located between the second and the third ionization chamber. The ATHENA software[30] was used to extract EXAFS oscillations. Experimental EXAFS spectra were Fourier transformed using a Hanning window over the k-range 2.8−12.5 $Å^{-1}$. The ARTEMIS software[30] was used for the curve fitting in k^3 space. Both the interatomic scattering path phases and amplitudes were calculated using the ab initio code FEFF8.20.[31] Data fitting was performed in k^3 space for R values ranging from 1.4 to 6.3 Å. The S_0^2 value was set at 0.90, and the shift in threshold energy was varied as a global parameter.

III. RESULTS AND DISCUSSION

Structure of $UC_{1\pm x}$ Materials. *III.1. Chemical Analysis: C, O, and N Content.* The chemical analyses made to determine the carbon, oxygen, and nitrogen content are summarized in Table 1. The uncertainty of the analyses is estimated at 3 wt %,

Table 1. Chemical Analysis of the $UC_{1\pm x}$

	$UC_{0.96}$	$UC_{1.00}$	$UC_{1.04}$
theoretical C content (wt %)	4.62	4.80	4.99
measured C content (wt %)	4.60 (14)	5.00 (15)	4.90 (15)
C/U ratio	0.96 (3)	1.04 (3)	1.02 (3)
O (ppm)	142 (30)	94 (19)	119 (24)
N (ppm)	<2	<2	<2

corresponding to an uncertainty in the stoichiometry of uranium carbides of about ±0.03. Because of this high uncertainty of the chemical analyses relative to the small changes in the carbon composition in the samples, it is difficult to give an absolute quantification of the C/U by this method. As expected with arc melting as a synthesis method, the oxygen content present in the samples is low and is significantly better than can be achieved using the carbothermoreduction method.

III.2. XRD. The XRD patterns of $UC_{1\pm x}$ ($1 \pm x = 0.96$, 1.00, and 1.04) samples are displayed in Figure 1. Two structural models can be suggested for the carbon position, NaCl ($Fm\bar{3}m$) or ZnS ($F\bar{4}3m$) types, in which the carbon atoms occupy the octahedral or the tetrahedral sites, respectively. Because of the low scattering factor of the carbon relative to the uranium atoms as well as the small range of C/U composition, Rietveld analysis using the X-ray diffraction pattern is not capable of defining the atomic positions of the carbon and its composition in the uranium carbides. Neutron diffraction could be more relevant for this purpose. In this study, XRD defines the quality

dx.doi.org/10.1021/ic402144g | Inorg. Chem. 2013, 52, 11669−11676

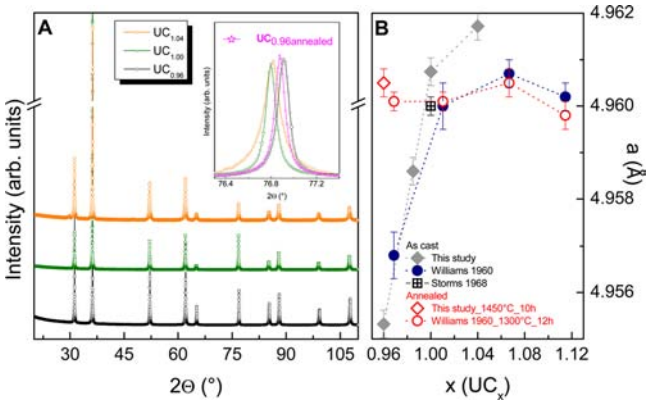

Figure 1. (A) XRD patterns of the $UC_{1\pm x}$ samples. The inset compares the (400) peak of $UC_{1\pm x}$ as-cast samples with a $UC_{0.96}$ annealed sample. (B) Lattice parameter (Å) evolution as a function of the C/U ratio.[34,33]

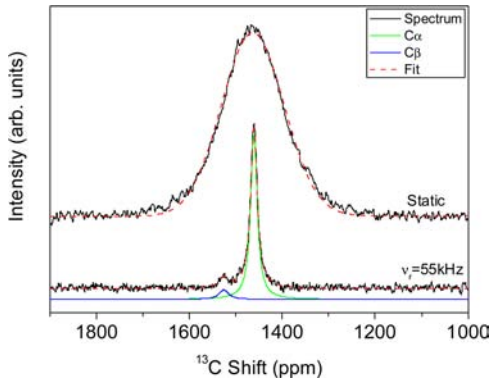

Figure 2. ^{13}C static Hahn-echo NMR spectrum of $UC_{1.00}$ (top). MAS Hahn-echo NMR spectrum and its corresponding fit (B_0 = 9.4 T and ν_r = 55 kHz) (bottom).

of the samples in terms of impurities and crystallinity. Thus, all of the samples displayed the fcc structure expected for uranium monocarbide and are highly crystalline, as shown by the narrow diffraction peaks. Because of the high quality of the measurement, a small peak around $2\theta = 35.6°$ has been detected in the $UC_{0.96}$ sample, which coincides with the highest intensity peak expected for free uranium metal with its orthorhombic structure. Actually, according to the U−C phase diagram,[32] U and UC coexist in the hypostoichiometric domain.

The lattice parameters of the $UC_{1\pm x}$ samples versus the C/U ratio are plotted in Figure 1 and are compared with previous values.[33,34,21] In agreement with the literature data, two evolutions of the lattice parameter with the C/U ratio are observed: for C/U < 0, there is a linear increase with the increasing C/U ratio and for C/U ≥ 0, the lattice parameter remains more constant. The inset in Figure 1 shows this evolution in terms of a single diffraction peak. Considering the low amount of oxygen assessed with the chemical analyses, the evolution of the lattice parameter cannot be attributed to the presence of oxygen impurity in these samples. In contrast, an increase of the oxygen content in U carbides leads to a decrease of the lattice parameter.[35] Even if oxygen is very difficult to detect by XRD, the fact that neither broad peaks nor a UO_2 phase are observed as well as the fact that the lattice parameter increases with carbon content suggests that the oxidation is very limited, in agreement with the chemical analyses. To support this statement, XRD measurements were also performed on the samples used for EXAFS experiments after 2 months storage, and no variation of the lattice parameter was detected, confirming the absence of sample oxidation.

III.3. NMR. The specially adapted NMR spectrometer available at the JRC-ITU allows unique, high-spinning-speed spectra of radioactive samples to be obtained. As the $UC_{1\pm x}$ are semimetals, large NMR resonance shifts (Knight shifts) are expected because of the collective hyperfine shifts of unpaired electrons near the Fermi surface of these materials.[36] In Figure 2, the static and the spinning Hahn echo spectra of the $UC_{1.00}$ sample are compared; the values obtained by fitting the spectra are reported in Table 2. First, the ^{13}C static spectrum is characterized by a broad Gaussian with a maximum at 1463 ppm and a full-width at half-maximum (fwhm) of 16 kHz (159 ppm). The absence of an anisotropic static line shape is consistent with the cubic symmetry around the ^{13}C nucleus. The line width is, thus, attributed to a range of shifts resulting from the paramagnetic susceptibility of the $UC_{1.00}$ particles and a distribution of local fields arising from the distribution of particle shapes in the powder. Spinning the sample at very high speed (ω_r = 55 kHz) results in a sharpening of the peak to give a high-resolution spectrum. This highly resolved spectrum is composed of one symmetric, purely Lorentzian peak with a chemical shift of 1461 ppm, similar to that observed in the ^{13}C static spectrum but with a fwhm almost 10 times narrower than that of the static. This is consistent with the octahedral local environment. A second small purely Lorentzian peak at 1526 ppm is also visible with 4% of the total signal intensity. Although in a first instance only one carbon environment is expected in $UC_{1.00}$, the ^{13}C MAS spectrum detects the presence of this second carbon environment, albeit in a very small quantity relative to the main peak. In the recent EXAFS study by Vigier et al.[19] on a $UC_{1.00}$ sample whose preparation and lattice parameter are similar the $UC_{1.00}$ sample in this study, the authors propose the presence of one type of carbon in the sample. In NMR, a chemically different, second carbon environment can be detected, even in low concentration. Indeed, only the achievement of a perfect crystal with a precise and exact stoichiometry of $UC_{1.00}$ can lead to one single-carbon environment. This would be quite an achievement and is challenging because of the difficulty of controlling the final composition of the uranium carbide samples by arc melting. Certainly, weight loss during this preparation can be limited but never avoided completely. The presence of a second carbon environment in hyperstoichiometric $UC_{1\pm x}$ could be expected and is now detected in the ^{13}C MAS spectrum. Thus, we argue that the main and purely Lorentzian peak observed in the ^{13}C spectrum can be attributed to carbons localized on the octahedral sites of the NaCl structure. The second and smaller Lorentzian peak is due to the presence of excess carbon present in the lattice. The Lorentzian nature of this peak suggests that it represents carbon in a well-defined 'defect environment'. This could be as either C−C dumbbells or C in the other tetrahedral interstitial positions in the NaCl structure. Previous density functional calculations[37,20] suggest that the first assumption, carbon in the form of a dumbbell, is preferred because of its lower energy of formation. These calculations indicate that the energy of formation of C_2 dumbbells having the ⟨111⟩ or ⟨110⟩ orientations is about 2.18 and 2.16 eV, respectively, whereas the formation energy of carbon in the interstitial position is equal to 2.52 eV.[37] The presence of a second peak with 4% intensity suggests that the true composition of the $UC_{1.00}$ is in fact

dx.doi.org/10.1021/ic402144g | *Inorg. Chem.* 2013, 52, 11669−11676

Table 2. ^{13}C Shift and Full-Width at Half-Maximum (FWHM) of the $UC_{1\pm x}$ Samples

	shift (ppm)		fwhm (ppm) spinning		fwhm (Hz) static	
compounds	$^{13}C\alpha$	$^{13}C_\beta$	$^{13}C\alpha$	$^{13}C_\beta$	$^{13}C\alpha$	$^{13}C_\beta$
$UC_{1.04}$	1463	1525	23.1 (2)	35.6 (2)	153.1 (4)	
$UC_{1.00}$	1461	1526	16.7 (2)	25.2 (2)	159.1 (4)	
$UC_{0.96}$	1448	1483	28.5 (4)	108.9 (2)	147.7 (6)	335.7(2)
	^{13}C					
$UC_{0.96\ annealed}$		1468	25.5 (3)		150.8 (7)	
$UC_{0.985}$	1458	1486	25.5 (3)	101.2 (2)	135.4(4)	292.5(1)

$UC_{1.02}$. This is because the introduction of a C−C dumbbell at the site of a C atom affects two carbon atoms, the original plus the excess carbon. Therefore, $UC_{1.02}$ would have 4% of C in these sites.

In Figure 3, the ^{13}C MAS spectra of $UC_{0.96}$, $UC_{0.985}$, and $UC_{1.04}$ are presented and compared with the $UC_{1.00}$ spectrum.

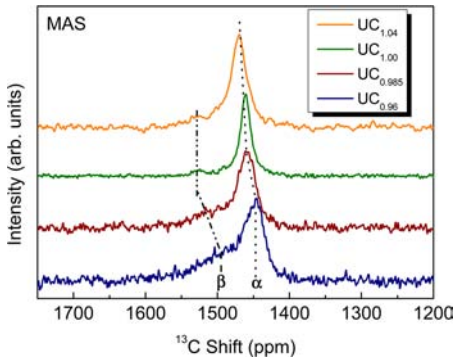

Figure 3. ^{13}C Hahn-echo MAS NMR spectra of $UC_{1.04}$, $UC_{1.00}$, $UC_{0.985}$, and $UC_{0.96}$ (B_0 = 9.4 T and ν_r = 55 kHz).

For all samples, two peaks are observed, the main, and sharper, one will be designated as the α peak, whereas the smaller and broader peak is reported as here as the β peak. Two effects can be observed and are defined by the substitution of excess carbon in the lattice in hyperstoichiometric samples as well as the absence of carbon from sites in hypostoichiometric $UC_{1\pm x}$. In the former, $UC_{1.00}$ and $UC_{1.04}$ samples exhibit an additional narrow peak at 1527 ppm, indicating the presence of a well-defined C defect site. In $UC_{1.04}$, there is also a small amount of additional intensity between these two resonances. In $UC_{0.985}$ and $UC_{0.96}$, broad additional peaks are observed at higher frequency in addition to peaks that are close to the peak for octahedral carbon in the UC lattice. One interpretation of the hypostoichiometric spectra would be that some UC, closer to perfect stoichiometry, is responsible for the sharper peak close to the $UC_{1.00}$ main peak (peak α) and that it is coexisting with more disordered material that produces the broader peaks at higher frequency (peak β). There appears to be a correlation between the increasing paramagnetic shift and peak broadening of the ^{13}C NMR line and the decreasing C content of the UC_{1-x}. The origin of this shift would require a detailed electronic structure calculation. However, because the magnitude of the shift is on the order of a hundred ppm for a very small change in C content, it is likely to be a Knight shift effect resulting from a change in the density of states at the Fermi level rather than a chemical shift effect. The width of the line is indicative of a range of these isotropic Knight shifts. It is clear that the MAS NMR can narrow a susceptibility-broadened line, and the origin of the broadening here is the distribution of local environments. The corresponding static spectrum of the $UC_{1\pm x}$ samples, not reported here because all are characterized by a broad Gaussian peak and the extracted shifts are in a good agreement with the previous ^{13}C static spectrum results reported by Lewis et al.,[38] were from a sample with a C/U ratio of 1.03.

The resonance shifts and the fwhm of the α and β MAS NMR peaks versus the composition of the uranium carbide samples are shown graphically in Figure 4. The trend of the

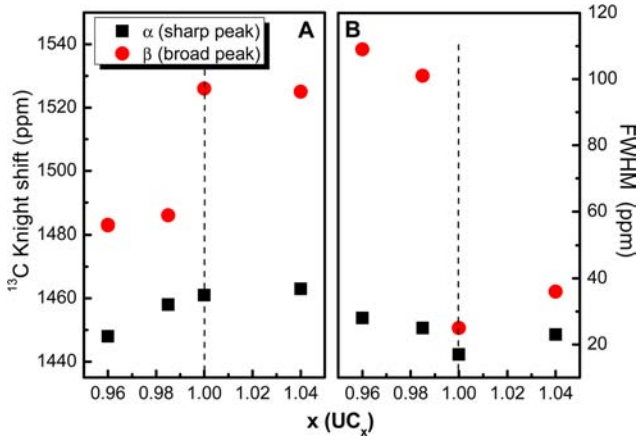

Figure 4. (A) Evolution of the ^{13}C NMR shift as a function of the C/U ratio. (B) Evolution of the fwhm as a function of the C/U ration. The dotted line at C/U = 1.00 indicates the transition from a high- to low-fwhm value, corresponding to a transition to more ordered sample.

shifts to higher frequencies for lower C contents are present for both peaks but are more emphasized for the β peak. One can assume that the broad β peaks in hypostoichiometric samples can be attributed to carbon atoms, which are surrounded by vacancies in the next carbon shell.[39] ^{13}C NMR is a potentially powerful probe of the change in carbon local environments in the transition from hypo- to hyperstoichiometric uranium carbides.

III.4. EXAFS. According to the above NMR results, two C environments are systematically observed for each $UC_{1\pm x}$ material. In the case of $UC_{0.96}$ and $UC_{0.98}$, the presence of vacancies might explain this. Regarding the $UC_{1.00}$ and $UC_{1.04}$, one can assume that there is an excess of carbon atoms located either in an interstitial or dumbbell position. Therefore, to investigate further these materials, the local structure around the U atoms was investigated by EXAFS in addition to the C environment, as studied by NMR.

The Figures 5 and 6 present the U L_{III} experimental k^3-weighted EXAFS spectra and the corresponding Fourier transforms (FTs) of the $UC_{0.96}$, $UC_{1.00}$, and $UC_{1.04}$ materials. Three intense peaks are observed in the FTs. The first at ∼2.0 Å is due to the first C shell, the second at ∼3.3 Å corresponds

dx.doi.org/10.1021/ic402144g | Inorg. Chem. 2013, 52, 11669−11676

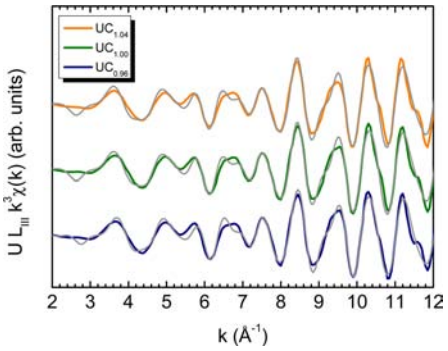

Figure 5. Experimental and fitted $k^3\chi(k)$ EXAFS spectra at the U L_{III} edge (the gray lines represent the fit).

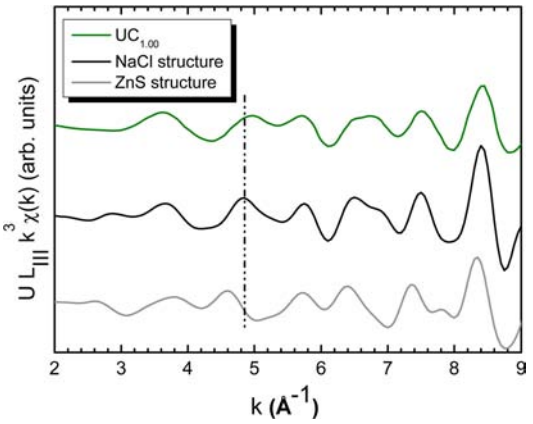

Figure 7. Experimental $k^3\chi(k)$ EXAFS spectrum of $UC_{1.00}$ compared with the simulated spectra based on the NaCl and ZnS structural types. The dotted line evidences the significant discrepancy between the NaCl structure of $UC_{1.00}$ and the ZnS structure.

mostly to the first U neighbor atoms, and the third peak at ~4.8 Å is attributed to multiple scattering paths.

As mentioned above, the NaCl-type structure was clearly established for $UC_{1.00}$,[19] but the ZnS structure ($F\bar{4}3m$) has not been completely discarded for nonstoichiometric $UC_{1\pm x}$ compounds. Although the XRD results of the present Article suggest that $UC_{0.96}$ and $UC_{1.04}$ actually have the rocksalt structure, EXAFS should be able to confirm this assumption; this method is more sensitive to the local atomic range than XRD. Thus, NaCl and ZnS structural-type EXAFS spectra of U were simulated with FEFF8.20[31] and are plotted in Figure 7. Significant discrepancies between NaCl- and ZnS-simulated EXAFS spectra are observed in the k range from 4 to 7 $Å^{-1}$. The oscillation at 4.8 $Å^{-1}$ is shifted significantly, as shown by the vertical line in Figure 7. The comparison of these data with the experimental data collected on the $UC_{1.04}$ sample confirms that the nonstoichiometric $UC_{1\pm x}$ exhibit the rocksalt structure too.

For all of the materials, one can assume that the presence of clustered defects can be discarded because no constant decrease of the amplitude of the experimental FTs EXAFS spectra is observed across the full R range. Actually, a particular amplitude decrease is observed at long distance. Indeed, the amplitude of the peaks does not decrease monotonically; this is particularly true for R values superior to 7.4 Å, where no peak can nearly be observed. This could support the presence of randomly distributed defects. Although the FTs are very similar, the region between 1.5 and 2.0 Å exhibits slight but, nevertheless, significant differences. Indeed, no peak is observed at ~1.8 Å for $UC_{0.96}$, whereas a small but distinct peak is detected at this distance for both the $UC_{1.00}$ and $UC_{1.04}$ samples. This suggests the presence of two first U−C distances instead of one, as would be expected in a perfect rocksalt structure. Furthermore, this bimodal environment is consistent with the two

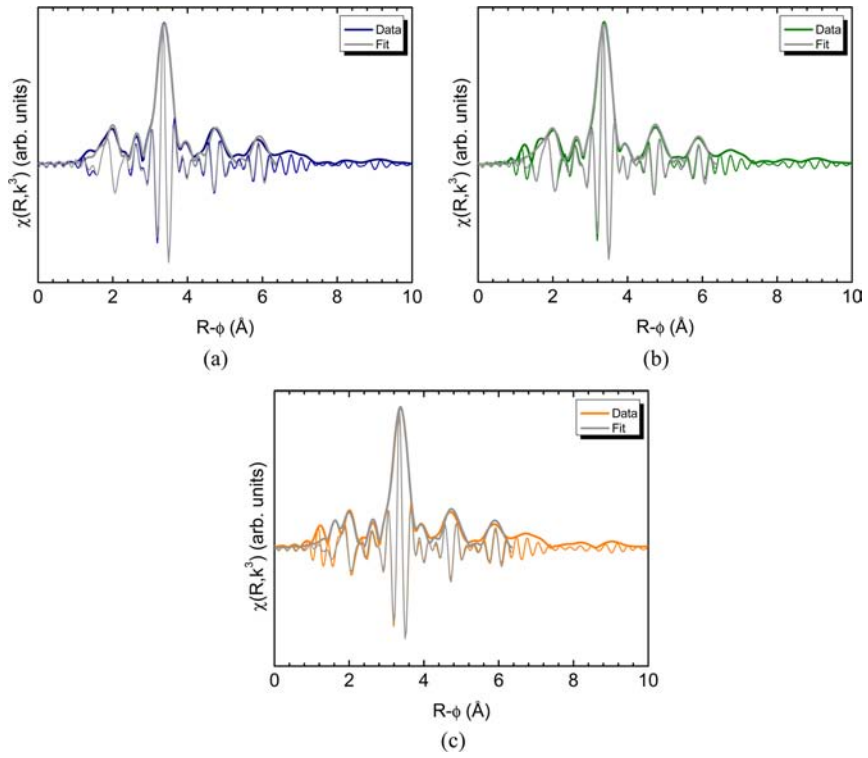

Figure 6. Modulus and real part of the Fourier transforms of k^3-weighted EXAFS spectra at the U L_{III} edge (a, $UC_{0.96}$; b, $UC_{1.00}$; and c, $UC_{1.04}$).

dx.doi.org/10.1021/ic402144g | Inorg. Chem. 2013, 52, 11669−11676

environments detected by NMR. Note that the peak amplitude increases with C content.

The splitting of the UC first neighbor shell is more apparent for the $UC_{1.04}$ sample. Figure 8 compares the experimental FT

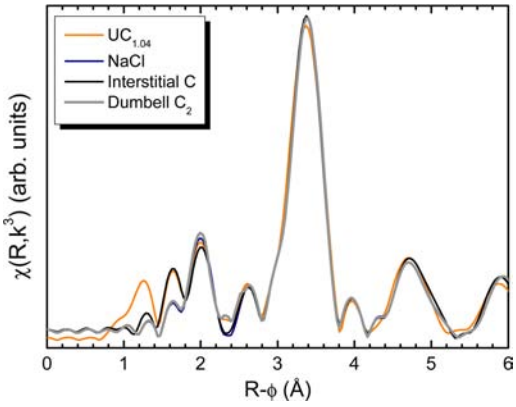

Figure 8. Modulus of Fourier transforms of $UC_{1.04}$ and fitted spectra using a perfect $Fm\bar{3}m$ structure type, a $Fm\bar{3}m$ structure type containing tetrahedral C interstitials, and a $Fm\bar{3}m$ structure containing C_2 dumbbells.

with various FTs calculated using different structural models. First, by considering a perfect NaCl-type structure for the data fitting, the small peak at ~1.8 Å is not replicated at all. Indeed, evidence for two C environments, with one of them being different than the NaCl structure, has been found, and it has been assumed that the carbon can therefore occupy either the interstitial or dumbbell position. Therefore, the presence of C_2 dumbbell pairs, as defects in the structure, has been considered. In the case of the fit with dumbbell, the best fit was achieved by considering a mixture of a pure NaCl structure and a NaCl structure with one dumbbell per unit. Various concentrations, configurations (α-UC_2[39,8] and β-UC_2[40]), and orientations ($\langle 110\rangle$, $\langle 111\rangle$[37]) have been taken into account. Figure 8 presents only the best result achieved including excess carbon in dumbbell configurations. One can note that the small peak at ~1.8 Å is still not replicated. On the basis of geometrical considerations, the presence of dumbbells in this type of material should result in the appearance of a multimodal distribution of the first U−C distance. The presence of carbon in interstitial positions was then considered, and a significant improvement of the fit was observed, especially in the 1.8 Å region, as shown in Figure 8. Using this structural model (NaCl structural with interstitial), the small peak is well fitted. Therefore, the present EXAFS study strongly suggests that excess carbon is accommodated on interstitial sites. As a consequence, the occupancy of such interstitial atomic positions was taken into account to fit the EXAFS spectra of $UC_{1.00}$ and $UC_{1.04}$.

In addition to the experimental data, Figures 5 and 6 present the calculated and fitted k^3-weigthed EXAFS spectra and the associated FTs. In the fitting procedure, a model cluster (NaCl type) with a lattice parameter of 4.96 Å was considered in the FEFF calculations. The coordination number of the first U−C shell was allowed to vary, but for the other shells this parameter was fixed according to the rocksalt structure. For $UC_{0.96}$, neither an additional distance nor an additional carbon position was included in the fitting procedure. For both $UC_{1.00}$ and $UC_{1.04}$, the presence of excess carbon in interstitial positions was permitted. Multiple scattering paths were considered, for example, triangular triple paths and quadruple paths from the C and U first neighbors. Table 3 summarizes the crystallographical parameters derived from the FEFF calculations. The low R-factor

Table 3. Crystallographic Parameters Derived from the U L_{III} EXAFS Spectra[a]

shell	R (Å)	N	σ^2 (Å^2)	R factor (%)
uranium carbide $UC_{0.96}$				1.9
U−C_1	2.47 (1)	5.7 (5)	0.008 (1)	
U−U_1	3.49 (1)	12	0.004 (1)	
U−C_2	4.15 (3)	8	0.009 (1)	
uranium carbide $UC_{1.00}$				1.8
U−C_{1a}	2.31 (1)	0.2 (5)	0.007 (1)	
U−C_{1b}	2.47 (1)	6.0 (5)	0.007 (1)	
U−U_1	3.50 (1)	12	0.004 (1)	
U−C_2	4.16 (2)	8	0.008 (1)	
uranium carbide $UC_{1.04}$				2.0
U−C_{1a}	2.31 (1)	0.9 (5)	0.007 (1)	
U−C_{1b}	2.48 (1)	6.0 (5)	0.007 (1)	
U−U_1	3.51 (1)	12	0.004 (1)	
U−C_2	4.16 (3)	8	0.008 (1)	

[a]R, interatomic distance; N, number of neighbors; σ^2, Debye−Waller factor; U−U_1, distance U−U in the first shell; U−C_{1a} and U−C_{1b}, first and second distance U−C in the first shell.

values (<2%) and the good agreement between experimental and fitted spectra confirm that the $UC_{1\pm x}$ compounds all have a NaCl structure.

In the case of hypostoichiometric $UC_{0.96}$, the first U−C_1 and U−U_1 distances are equal to 2.47 (1) and 3.49 (1) Å, respectively. Note that metallic U atoms found in XRD are not detected in the EXAFS analysis, possibly because it is a very minority phase. Regarding the $UC_{1.00}$ material, the U−C_1 and U−U_1 first interatomic distances are consistent with those already determined by an earlier EXAFS study[19] and by neutron diffraction (U−C_1 = 2.48 and U−U = 3.50 Å[19]). However, evidence for an additional U−C first-shell distance, denoted as UC_{1a} in Table 3, has been found in the present work. This bond length at 2.31 Å, as explained above, is attributed to the presence of excess carbon atoms in interstitial positions in the NaCl structure. For the hyperstoichiometric $UC_{1.04}$, two U−C first distances are observed as well; the U−C_{1a} and U−C_{1b} distances are 2.31 (1) and 2.48 (1) Å, respectively. The slight increase of the U −C_{1b} distance is in agreement with the slight increase of the lattice parameter and can be understood from the hyperstoichiometry.

III.5. Annealing of $UC_{0.96}$. The hypostoichiometric sample of $UC_{0.96}$ exhibits vacancies in the fcc carbon sublattice. The corresponding NMR spectrum exhibits a sharper peak at 1448 ppm with a width of 28.7 ppm and a broader peak centered at 1483 ppm that is 110 ppm wide. The sharp peak is attributed to C in a UC octahedral environment, and the broader peak is attributed to carbons in a UC octahedral site. There appear to be a fewer vacancies associated with the carbons in the sharper peak and more vacancies associated with the broader peak in a more disordered arrangement. Thus, the stoichiometry of this disordered material would be lower than 0.96, and the sharper peak would be closer to true stoichiometry. Assuming a 1.00 stoichiometry for the sharp peak and weighting by the areas under the two peaks, this stoichiometry would be 0.92. However, the shift of 1448 ppm, compared with 1461 ppm for $UC_{1.00}$, may even indicate a slightly carbon-rich region associated with this peak. Previous resistivity measurements have

dx.doi.org/10.1021/ic402144g | Inorg. Chem. 2013, 52, 11669−11676

shown that annealing quenched nonstoichiometric UC_{1-x} samples, leading to an ordering in the sample and has been explained by a reorganization of the vacancies.[41] Therefore, an annealing on the $UC_{0.96}$ sample was performed to confirm the link, in NMR spectra, between line broadening and disorder in the lattice. In the XRD patterns, the annealing of the sample leads to an increase of the lattice parameter (Figure 1) resulting from stress release, which is agreement with earlier literature observations.[34,6]

The NMR spectra of the annealed and of the as-cast $UC_{0.96}$ sample are presented in Figure 9. After heat treatment, the

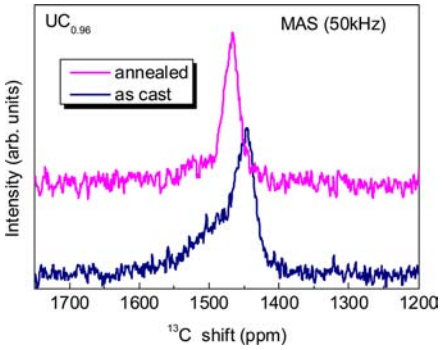

Figure 9. ^{13}C Hahn-echo MAS NMR spectra of $UC_{0.96}$ as-cast and $UC_{0.96}$ annealed at 1450 °C during 10 h (B_0 = 9.4 T and ν_r = 55kHz).

majority of the sample has transformed to yield a main Lorentzian ^{13}C peak with a fwhm of 25.7 ppm at 1468 ppm. A small broad peak (fwhm = 89.3 ppm) remains at 1481 ppm, but it is clearly in the noise. Hence, ^{13}C NMR indicates that the heat treatment has induced a substantial rearrangement of the carbon atoms across carbon-deficient and carbon-rich (possibly excess carbon) regions to produce one fairly uniform carbon environment with respect to vacancy ordering, as has been reported elsewhere.[42] The Lorentzian peak of the annealed $UC_{0.96}$ sample has a shift corresponding to the weighted average of the two peaks of the as-cast sample. Matsui et al.[6] have shown that the resistivity of the as-cast and hypostoichiometric samples ($UC_{0.98}$ and $UC_{0.96}$) is higher than for annealed samples, which they explained by the presence of stress and by the distribution of vacancies[43] in the lattice.[39] In this study, unlike XRD, the ^{13}C NMR spectra enable the observation of the transition from the disordered (as-cast) to the ordered (annealed) sample by virtue of the broadening and position of the peaks (Figure 9).

IV. SUMMARY

In the present work, the local carbon environments of $UC_{1\pm x}$ samples ($0.96 \leq 1 \pm x \leq 1.04$) were investigated using a unique combination of techniques: XRD, NMR, and EXAFS. To complement the long-range order analysis with XRD (structure and lattice parameters), both NMR and EXAFS are sensitive to short-range order distance (interatomic distances and coordination numbers). XRD showed an evolution of the lattice parameter versus carbon content. EXAFS indicates the NaCl-type structure was achieved for all compositions, distinctly excluding the ZnS structure. Also, EXAFS detects the presence of vacancies in the C sublattice and the full occupation of the U sublattice in the $UC_{0.96}$ sample. High-resolution ^{13}C MAS NMR spectra exhibit two peaks corresponding to two types of carbon environment in the lattice for all of the as-cast samples independently of the composition. The preparation of pure uranium monocarbide $UC_{1.00}$ is not achievable, at least by this synthesis method. By coupling NMR and EXAFS, it was possible to show that the two environments could be attributed to a majority C-atom sublattice in octahedral sites and to the excess of carbon atoms, which, according to the EXAFS analysis, is preferentially in interstitial positions. The transition from a disordered to an ordered structure in $UC_{1\pm x}$ samples has been observed by MAS NMR. The carbon content affects the broadening of the ^{13}C peaks, showing a sharp difference between hypo- and hyperstoichiometric samples. The presence and the heterogeneous distribution of vacancies in the as-cast hypostoichiometric samples leads to a broadening of the ^{13}C peaks. Only annealing could lift this disorder and provide a more ordered structure with the presence of a single ^{13}C peak as well as lead a lattice parameter closer to that found for a C/U ratio of 1.00, as displayed by XRD. Coupling NMR and EXAFS to XRD is powerful means to provide detailed unambiguous assignment of local structure. Unfortunately, the ^{235}U NMR active isotope has a low Larmor frequency and large quadrupole moment, making it unfavorable for high-resolution NMR, but the recent discovery of the ^{239}Pu NMR signal[44] bodes well for an even more powerful combination of these methods, whereby NMR and EXAFS can be used to probe identical nuclei.

AUTHOR INFORMATION

Corresponding Author

*E-mail: rrsula.carvajal-nunez@ec.europa.eu.

Notes

The authors declare no competing financial interest.

ACKNOWLEDGMENTS

We thank D. Bouxière, C. Boshoven, and S. Morel for sample preparation and for their technical help. We are also grateful to ANKA for providing beam time, and we especially thank K. Dardenne and J. Rothe for their support during the XAS experiments. We thank the referees for helpful comments.

REFERENCES

(1) Frost, B. R. T. *J. Nucl. Mater.* **1963**, *10*, 265−300.
(2) Kolokol, A. S.; Shimkevich, A. L. In *Proceedings of the International Conference on Nuclear Engineering*; Americna Society of Mechanical Engineers: New York, **2008**; Vol. *1*, pp. 759−763.
(3) Meyer, M. K.; Fielding, R.; Gan, J. *J. Nucl. Mater.* **2007**, *371*, 281−287.
(4) Matsui, H. *J. Nucl. Sci. Technol.* **1972**, *9*, 185−186.
(5) Le Guyadec, F.; Rado, C.; Joffre, S.; Coullomb, S.; Chatillon, C.; Blanquet, E. *J. Nucl. Mater.* **2009**, *393*, 333−342.
(6) Matsui, H.; Horiki, M.; Kirihara, T. *J. Nucl. Sci. Technol.* **1981**, *18*, 922−929.
(7) Sisman, O.; Morgan, J. G. *Irradiation Behaviour of High-Temperature Fuel Material*; Reactor Chemistry Division Annual Progress Report: Oak Ridge, TN, March 1968; pp 102−112.
(8) Akhachinskii, V. V.; Bashlykov, S. N. *At. Energy* **1969**, *27*, 1317−1326.
(9) Lee, H. M.; Barbett, L. R. *J. Nucl. Mater.* **1968**, *27*, 275−284.
(10) Watanabe, H.; Kikuchi, T.; Furukawa, K. *J. Nucl. Mater.* **1972**, *43*, 321−329.
(11) Menzies, I. A.; Strafford, K. N. *J. Nucl. Mater.* **1967**, *21*, 287−301.
(12) Gray, R. J.; Thurber, W. C.; DuBose, C. K. H. *Preparation and Metallography of Arc-Melted Uranium Carbides*; Oak Ridge National Laboratory: Oak Ridge, TN, 1958
(13) Tagawa, H.; Fujii, K.; Sasaki, Y. *J. Nucl. Sci. Technol.* **1971**, *8*, 244−249.

(14) Rodriguez, P. *Bull. Mater. Sci.* **1999**, *22*, 215−220.
(15) Mukerjee, S. K.; Dehadraya, J. V.; Vaidya, V. N.; Sood, D. D. *J. Nucl. Mater.* **1990**, *172*, 37−46.
(16) Maruya, K. *J. Nucl. Sci. Technol.* **1970**, *7*, 13−18.
(17) Catlow, C. R. A. *J. Nucl. Mater.* **1976**, *60*, 151−157.
(18) Rundle, R. E. *Acta Crystallogr.* **1948**, *1*, 180−187.
(19) Vigier; Den Auwer, C.; Fillaux, C.; Maslennikov, A.; Noël, H.; Roques, J.; Shuh, D. K.; Simoni, E.; Tyliszczak, T.; Moisy, P. *Chem. Mater.* **2008**, *20*, 3199−3204.
(20) Ducher, R.; Dubourg, R.; Barrachin, M.; Pasturel, A. *Phys. Rev. B* **2011**, *83*, 104107-1−104107-12.
(21) Matsui, H.; Matzke, H. *J. Nucl. Mater.* **1980**, *88*, 317−321.
(22) Harrison, J. W. *J. Nucl. Mater.* **1969**, *30*, 319−323.
(23) Colby, L. J., Jr. *J. Less-Common Met.* **1966**, *10*, 425−431.
(24) Schürenkämper, A. *J. Inorg. Nucl. Chem.* **1970**, *32*, 417−429.
(25) Farnan, I.; Cho, H.; Weber, W. J.; Scheele, R. D.; Johnson, N. R.; Kozelisky, A. E. *Rev. Sci. Instrum.* **2004**, *75*, 5232−5236.
(26) Slichter, C. P. *Principles of Magnetic Resonance*; Springer-Verlag: New York, 1980.
(27) Morcombe, C. R.; Zilm, K. W. *J. Magn. Reson.* **2003**, *162*, 479−486.
(28) Massiot, D.; Fayon, F.; Capron, M.; King, I.; Le Calvé, S.; Alonso, B.; Durand, J.-O.; Bujoli, B.; Gan, Z.; Hoatson, G. *Magn. Reson. Chem.* **2002**, *40*, 70−76.
(29) Rothe, J.; Butorin, S.; Dardenne, K.; Denecke, M. A.; Kienzler, B.; Löble, M.; Metz, V.; Seibert, A.; Steppert, M.; Vitova, T.; Walther, C.; Geckeis, H. *Rev. Sci. Instrum.* **2012**, *83*, 043105-1−043105-13.
(30) Ravel, B.; Newville, M. *J. Synchrotron Rad.* **2005**, *12*, 537−541.
(31) Rehr, J. J.; Ankudinov, A.; Zabinsky, S. I. *Catal. Today* **1998**, *39*, 263−269.
(32) Manara, D.; De Bruycker, F.; Sengupta, A. K.; Agarwal, R.; Kamath, H. S. In *Comprehensive Nuclear Materials*; Konings, R., Ed.; Elsevier: Oxford, 2012; pp 87−137.
(33) Storms, E. K.; Huber, E. J., Jr. *J. Nucl. Mater.* **1967**, *23*, 19−24.
(34) Williams, J.; Sambell, R. A. J.; Wilkinson, D. *J Less-Common Met.* **1960**, *2*, 352−356.
(35) Potter, P. E. *J. Nucl. Mater.* **1972**, *42*, 1−22.
(36) Levine, S. G. *J. Chem. Educ.* **2001**, *78*, 133.
(37) Freyss, M. *Phys. Rev. B* **2010**, *81*, 014101-1−014101-16.
(38) Lewis, W. B.; Rabideau, S. W.; Krikorian, N. H.; Witteman, W. G. *Phys. Rev.* **1968**, *170*, 455−462.
(39) Sarian, S.; Dalton, J. T. *J. Nucl. Mater.* **1973**, *48*, 351−359.
(40) Chartier, A.; Van Brutzel, L. *Nucl. Instrum. Methods Phys. Res., Sect. B* **2007**, *255*, 146−150.
(41) Storms, E. K. *Analytical Representation of the Thermal Conductivity and Electrical Resistivity of* $UC_{1\pm x}$, PuC_{1-x}, *and* $(U_yPu_{1-y})C_{1\pm x}$; Technical Report for Los Alamos National Laboratory: Los Alamos, NM, 1982
(42) Kim, N.; Stebbins, J. F. *Chem. Mater.* **2007**, *19*, 5742−5747.
(43) Hisayuki, M.; Ken-ichi, S.; Mitsuo, I.; Hiromi, A.; Tomoo, K. *J. Nucl. Mater.* **1975**, *57*, 93−97.
(44) Yasuoka, H.; Koutroulakis, G.; Chudo, H.; Richmond, S.; Veirs, D. K.; Smith, A. I.; Bauer, E. D.; Thompson, J. D.; Jarvinen, G. D.; Clark, D. L. *Science* **2012**, *336*, 901−904.